Journal of Materials Chemistry C

Deep red emission in Eu2+-activated Sr4(PO4)2O phosphors for blue-pumped white LEDs

Journal:	*Journal of Materials Chemistry C*
Manuscript ID:	TC-ART-04-2015-001151.R1
Article Type:	Paper
Date Submitted by the Author:	02-Jun-2015
Complete List of Authors:	KOMURO, NAOYUKI; Mitsubishi Chemical Corporation, Phosphor R&TD center Mikami, Masayoshi; MCHC R&D Synergy Center, Inc., Saines, Paul; The University of Oxford, Inorganic Chemistry Laboratory Akimoto, Katsuhiro; University of Tsukuba, Institute of Applied Physics Cheetham, Tony; University of Cambridge, Department of Materials Science and Metallurgy

Journal of
Materials Chemistry C

RSCPublishing

ARTICLE

Deep red emission in Eu^{2+}-activated $Sr_4(PO_4)_2O$ phosphors for blue-pumped white LEDs

Cite this: DOI: 10.1039/x0xx00000x

Naoyuki Komuro[*a,d], Masayoshi Mikami[b], Paul J. Saines[c], Katsuhiro Akimoto[d] and Anthony K. Cheetham[e]

Received ooth January 2012,
Accepted ooth January 2012

DOI: 10.1039/x0xx00000x

www.rsc.org/MaterialsC

The deep red phosphor $Sr_4(PO_4)_2O:Eu^{2+}$, which has an excitation peak around 450 nm for blue LED applications, is reported. This behavior is unusual for most phosphate phosphors. The crystal structure of $Sr_4(PO_4)_2O:Eu^{2+}$ is found to be monoclinic $P2_1$ and isotypic with $Ca_4(PO_4)_2O:Eu^{2+}$, which also shows deep red emission. $Sr_4(PO_4)_2O:Eu^{2+}$ has a larger lattice volume than $Ca_4(PO_4)_2O:Eu^{2+}$, but their emission and excitation spectra at room temperature are very similar. The key factors are discussed for achieving a large redshift of the 5*d* levels of Eu^{2+} ion in order to emit red light. In particular, the importance of the anion polarizability and the distortions of the metal coordination polyhedra are discussed, including the effective coordination number. Importantly, $Sr_4(PO_4)_2O:Eu^{2+}$ lacks the yellow emission at 77 K, which is found in $Ca_4(PO_4)_2O:Eu^{2+}$. The differences in thermal quenching behavior for Eu^{2+} dopants in $Sr_4(PO_4)_2O:Eu^{2+}$ and $Ca_4(PO_4)_2O:Eu^{2+}$ are attributed to the degree of auto/photo-ionization due to differences in the band gaps of these compounds. The importance of the large band gap of the host lattice in avoiding non-radiative processes of energy relaxation was confirmed.

1 Introduction

White light-emitting diodes (LEDs) consisting of an InGaN LED and phosphors have been intensively developed for solid-state lighting (SSL) with high luminous efficiency and good color quality. The replacement of conventional lighting sources by LEDs has accelerated in recent years, driven by the requirement to reduce consumption of both energy and resources. The development of phosphors has been contributing to this since the fabrication of white LEDs currently relies on the use of phosphors to convert high energy blue or near-ultraviolet (UV) LED light into lower energy visible light.[1, 2] Currently, the most common approach for white LEDs is to combine a blue LED with a color-converting phosphor, first achieved using a $YAG:Ce^{3+}$ phosphor for blue-to-yellow down conversion. There are few examples of new phosphate phosphors that exhibit good excitation and emission performance when combined with blue LEDs. Lagos reported the behavior of α-$Sr_2P_2O_7:Eu^{2+}$ and α-$Sr_3(PO_4)_2:Eu^{2+}$ as blue phosphors and α-$Ca_3(PO_4)_2:Eu^{2+}$ as a green phosphor for UV excitation.[3] $CaZr(PO_4)_2:Eu^{2+}/Eu^{3+}$ was also reported for deep UV excitation.[4] However these materials are poorly matched to blue LEDs.

We have previously reported $Ca_6BaP_4O_{17}:Eu^{2+}$,[5] which is a rare bright yellow phosphor that can be excited using blue light and is importantly the first example reported in a phosphate system. We have also reported that $Ca_4(PO_4)_2O:Eu^{2+}$ (hereafter referred to as $TTCP:Eu^{2+}$), which has the longest excitation wavelength amongst phosphate systems, emits deep red light at room temperature and considerably broad emission from 500 nm to 800 nm at 77 K.[6] The relationship between the crystal structure and the unique emission characteristics of $TTCP:Eu^{2+}$ was discussed, differentiating the eight Ca sites. The importance of the anion polarizability and the distortions of the coordination polyhedra were also highlighted.

We report herein the crystal structure and the emission characteristics of $Sr_4(PO_4)_2O:Eu^{2+}$ (hereafter referred to as $TTSP:Eu^{2+}$) as a new red phosphor well matched to blue LEDs. Despite previously reported difficulties in the synthesis of $Sr_4(PO_4)_2O$ leading to the formation of an apatite phase,[7] we managed to find optimal conditions to synthesize $Sr_4(PO_4)_2O:Eu^{2+}$. $Sr_4(PO_4)_2O$ is chemically stable under ambient condition without reacting with moisture. The crystal structure of $TTSP:Eu^{2+}$ is isotypic with the structure of $TTCP:Eu^{2+}$. The emission efficiency of $Sr_4(PO_4)_2O:Eu^{2+}$ is not high due to non-radiative relaxation, which is attributed to photo-ionization, as we discuss in this work. However, it is important to understand the key factors that allow Eu^{2+} to exhibit a large redshift in phosphors, and these are discussed in the context of anion polarizability and the distortions of the coordination polyhedra around Eu^{2+} in $TTSP:Eu^{2+}$ and $TTCP:Eu^{2+}$. The determining factor for the radiative/non-radiative energy relaxation processes in $TTSP:Eu^{2+}$ and $TTCP:Eu^{2+}$ was revealed by comparing their band gaps.

2 Experimental

A sample of $TTSP:Eu^{2+}$ was synthesized by conventional solid-state reaction of $SrCO_3$ (Hakushin Chemicals), $SrHPO_4$(Alfa Aesar) and Eu_2O_3(Alfa Aesar). Stoichiometric mixtures of the raw materials were placed in alumina crucibles and heated in a reducing atmosphere of $5\%H_2 + 95\%N_2$ at 1450°C for 5hrs. After the synthesis, the samples were ground into fine powders for characterization. Synchrotron X-ray diffraction data were collected on beamline I11 at the Diamond Light Source facility in the UK using a wavelength of 0.82713 Å.[8] Structure

refinement was performed by the Rietveld method using the program GSAS.[9, 10] The crystal structure of TTSP:Eu^{2+} was depicted in VESTA, in which the effective coordination numbers (ECoNs) were also calculated.[11] Photoluminescence (PL) and photoluminescence excitation (PLE) spectra at room temperature were measured using a JASCO FP-6500 spectrometer and at 77 K using a Horiba FluoroLog-3 spectrometer. The UV-vis reflectance spectra were measured using a PerkinElmer Lambda 750 spectrophotometer. To evaluate the band gap of TTSP, density functional theory (DFT) calculations with a hybrid nonlocal exchange-correlation functional (HSE) were performed using the Vienna Ab initio Simulation Package (VASP) code. The electron−ion interaction was described by the projector augmented wave (PAW) method. The basis set cutoff was 400 eV.[12, 13, 14]

3 Results and discussion

3.1 The structure refinement of $Sr_4(PO_4)_2O:Eu^{2+}$

The crystal structure of TTSP:Eu^{2+} was originally reported as orthorhombic in space group $P222_1$ by Bauer.[15] The structure in this work was found to be a monoclinic, having space group $P2_1$ slightly distorted from $P222_1$, and is isotypic with the structure of TTCP:Eu^{2+}. Fig. 1 shows the high quality of the Rietveld fit to the X-ray synchrotron powder diffraction pattern obtained of TTSP:Eu^{2+} using the monoclinic $P2_1$ structure. The refinement using the orthorhombic $P222_1$ structure showed worse fits. Rietveld refinements revealed that the sample contained a relatively small amount of a $Sr_{10}(PO_4)_6O$ impurity, 10.1(6)% by weight. However, since $Sr_{10}(PO_4)_6O:Eu^{2+}$ is unable to be excited by visible light, this factor is negligible for our discussion of the optical properties of $Sr_4(PO_4)_2O:Eu^{2+}$.[16]

Table 1 shows structural parameters for TTSP:Eu^{2+}, including R indexes of R_{wp} = 9.2% and R_p = 7.2%, and compares them with the parameters of TTCP:Eu^{2+} from our previous work. TTSP:Eu^{2+} has a monoclinic structure in space group $P2_1$ with lattice parameters a = 7.390703(9) Å, b = 12.58826(2) Å, c = 9.82929(1) Å and 90.5797(1)º. The crystal structure is illustrated in Fig. 2 and the atomic coordinates of are shown in Table 2. Seven of the Sr sites are coordinated by seven oxygen atoms with an average bond length from 2.60 Å to 2.68 Å, and one Sr site (Sr8) is coordinated by six oxygen atoms with an average bond length of 2.54 Å. The refined sample contained 0.5mol% Eu^{2+}, but it was not possible to determine the distribution of Eu^{2+} ions over the cation sites by structural refinement. Bond valence sums were calculated to confirm the proper coordination numbers and oxidation states.[17] Bond distances from the divalent cations in the TTSP structure, the bond valence sums and ECoNs are listed in Table 3. The four P sites are in PO_4 tetrahedra which are isolated from other PO_4 tetrahedra. The structure also contains two distinct oxide anions that are not part of a PO_4 tetrahedron (labeled O17 and O18).

Table 1 Crystallographic data and structure refinement for TTSP:Eu^{2+}.

	TTSP (This work)	TTCP (Previous work)	TTSP (Bauer)
Unit cell	a = 7.390703(9) Å b = 12.58826(2) Å c = 9.82929(1) Å β = 90.5797(1) º	a = 7.01444(5) Å b = 11.9792(1) Å c = 9.46490(7) Å β = 90.8915(4) º	a = 7.38 Å b = 12.57 Å c = 9.79 Å β = 90 º
Cell volume	V = 914.431(2) Å^3	V = 795.22(1) Å^3	V = 908.19 Å^3
Space group	$P2_1$	$P2_1$	$P222_1$
R indexes	R_{wp} = 9.2% R_p= 7.2% χ^2 = 1.4		

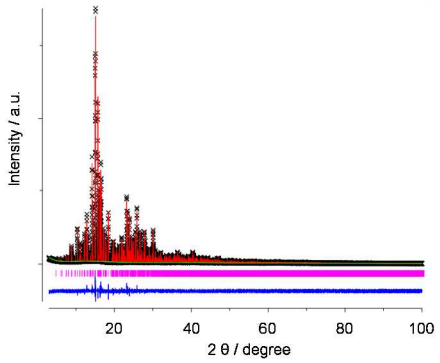

Fig. 1 Synchrotron x-ray powder diffraction pattern of TTSP:Eu^{2+}.. The crosses, and upper and lower continuous lines are the experimental, calculated and difference profiles, respectively; the vertical lines are the allowed Bragg reflections markers.

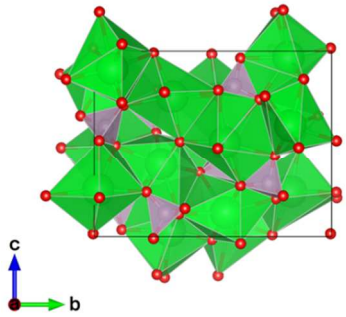

Fig. 2 Schematic crystal structure illustration of TTSP:Eu^{2+} projected onto the (100) plane. Sr, P and O atoms are shown as green, mauve and red spheres.

Table 2 Atomic parameters of $Sr_4(PO_4)_2O$ with all sites in the refinement being set to be fully occupied.

Atom	Site	x	y	z
Sr1	2a	0.53266(21)	0.28092(16)	0.39346(16)
Sr2	2a	0.03391(20)	0.32596(16)	0.39863(15)
Sr3	2a	0.25916(21)	0.31862(17)	0.03204(16)
Sr4	2a	0.24033(21)	0.82807(15)	0.24306(16)
Sr5	2a	0.75540()	0.01706(15)	0.25294(16)
Sr6	2a	0.24835(23)	0.04954(17)	0.48861(14)
Sr7	2a	0.49668(21)	0.55413(16)	0.12994(15)
Sr8	2a	0.01624(21)	0.57569(15)	0.09355(15)
O1	2a	0.2379(14)	0.1162(4)	0.7254(9)
O2	2a	0.1079(10)	0.2961(6)	0.7808(8)
O3	2a	0.4318(10)	0.2645(7)	0.7965(9)
O4	2a	0.2748(14)	0.2600(7)	0.5625(6)
O5	2a	0.7854(14)	0.2196(6)	0.2405(8)
O6	2a	0.6081(9)	0.3566(7)	0.1223(10)
O7	2a	0.9389(10)	0.3822(6)	0.1508(9)
O8	2a	0.1660(12)	0.7498(7)	0.0104(6)
O9	2a	0.2770(13)	0.1169(7)	0.0373(6)
O10	2a	0.4116(10)	0.0198(6)	0.2383(8)
O11	2a	0.0898(9)	0.0219(6)	0.2091(8)
O12	2a	0.2546(15)	0.1947(5)	0.2589(9)
O13	2a	0.0938(9)	0.5205(7)	0.4797(8)
O14	2a	0.3293(12)	0.4431(5)	0.3456(9)
O15	2a	0.2303(14)	0.6238(6)	0.2881(8)
O16	2a	0.5929(10)	0.0890(7)	0.4937(7)
O17	2a	0.7630(13)	0.3616(8)	0.5170(10)
O18	2a	0.7395(13)	-0.0046(7)	0.0157(9)
P1	2a	0.2622(6)	0.23607(32)	0.7140(4)
P2	2a	0.7903(5)	0.30030(31)	0.1251(4)
P3	2a	0.2577(6)	0.08866(31)	0.1861(4)
P4	2a	0.2664(5)	0.54795(33)	0.4054(4)

Table 3 Bond distances, bond valence sums and ECoNs of $Sr_4(PO_4)_2O$

Bond	Distance (Å)	Bond Valence	Bond	Distance (Å)	Bond Valence
Sr1_O17	2.316	0.586	Sr5_O18	2.350	0.534
Sr1_O5	2.530	0.328	Sr5_O11	2.514	0.343
Sr1_O4	2.555	0.307	Sr5_O10	2.544	0.316
Sr1_O14	2.576	0.290	Sr5_O5	2.562	0.301
Sr1_O16	2.645	0.241	Sr5_O16	2.814	0.152
Sr1_O12	2.664	0.229	Sr5_O13	2.844	0.141
Sr1_O6	2.891	0.124	Sr5_O2	2.980	0.097
Total		**2.104**	Total		**1.885**
ECoN		**5.6**	ECoN		**5.0**
Bond	Distance (Å)	Bond Valence	Bond	Distance (Å)	Bond Valence
Sr2_O17	2.368	0.509	Sr6_O17	2.368	0.509
Sr2_O4	2.529	0.329	Sr6_O1	2.476	0.380
Sr2_O13	2.612	0.263	Sr6_O13	2.577	0.289
Sr2_O7	2.626	0.253	Sr6_O16	2.595	0.275
Sr2_O14	2.690	0.213	Sr6_O4	2.754	0.179
Sr2_O12	2.706	0.204	Sr6_O10	2.777	0.168
Sr2_O5	2.743	0.185	Sr6_O12	2.905	0.119
Total		**1.956**	Total		**1.920**
ECoN		**6.1**	ECoN		**5.7**
Bond	Distance (Å)	Bond Valence	Bond	Distance (Å)	Bond Valence
Sr3_O18	2.274	0.656	Sr7_O18	2.365	0.513
Sr3_O9	2.544	0.316	Sr7_O9	2.486	0.370
Sr3_O2	2.715	0.199	Sr7_O1	2.534	0.325
Sr3_O12	2.722	0.195	Sr7_O6	2.621	0.257
Sr3_O3	2.740	0.186	Sr7_O15	2.669	0.226
Sr3_O6	2.760	0.176	Sr7_O3	2.794	0.161
Sr3_O7	2.768	0.173	Sr7_O14	2.834	0.144
Total		**1.902**	Total		**1.995**
ECoN		**4.4**	ECoN		**5.7**
Bond	Distance (Å)	Bond Valence	Bond	Distance (Å)	Bond Valence
Sr4_O17	2.397	0.470	Sr8_O18	2.340	0.549
Sr4_O8	2.545	0.315	Sr8_O15	2.543	0.317
Sr4_O3	2.585	0.283	Sr8_O9	2.562	0.301
Sr4_O15	2.611	0.264	Sr8_O7	2.566	0.298
Sr4_O2	2.613	0.262	Sr8_O8	2.591	0.278
Sr4_O11	2.701	0.207	Sr8_O1	2.650	0.237
Sr4_O10	2.725	0.194			
Total		**1.996**	Total		**1.981**
ECoN		**6.4**	ECoN		**5.5**

3.2 Optical properties of $Sr_4(PO_4)_2O:Eu^{2+}$

Fig. 3 shows the PL and PLE spectra of TTSP:Eu^{2+} at different Eu concentrations with respect to Sr, excited at 465 nm and monitored at 680 nm at room temperature. TTSP:Eu^{2+} has a broad red emission spectrum with a peak position at 695 nm and a full width at half maximum of 170 nm. The emission at 695 nm corresponds to the $4f^6 5d^1 - 4f^7$ transition of the Eu^{2+} ions. The Stokes shift is estimated as around 6300 cm^{-1} and the color coordinates on the CIE chromaticity diagram are (0.648, 0.350). The emission intensity of TTSP:Eu^{2+} initially increases with higher Eu doping due to significantly enhanced absorbance, reaches a maximum at x = 0.005 (0.5mol%), and then decreases, resulting from the concentration

quenching. The asymmetric emission spectra of TTSP:Eu^{2+} can be deconvoluted and ascribed to up to eight different emission sites, which could be identified as the different coordination environments of Sr^{2+} ions being occupied by Eu^{2+} ions. However it was found to be difficult to relate the deconvoluted Gaussian components to the different coordination environments of Eu^{2+} ions at Sr sites. As discussed later, Eu^{2+} ions in some Sr sites of TTSP seem not to contribute to the emission spectra of TTSP:Eu^{2+}, presumably due to non-radiative relaxation processes of Eu^{2+} ions in some of the Sr sites. As mentioned above, it was not possible to determine the distribution of Eu^{2+} ions over the cation sites by powder X-ray diffraction data (PXRD) due to the large number of Sr sites in TTSP, but we believe that this ion uniformly substitutes at eight Sr sites for doping levels over 0.5mol%. Normally, different Eu^{2+} ions distribution across several cation sites with different crystal field environments can change the emission spectrum depending on the contribution from each site. However, the spectral shapes from samples with over 0.5mol% doping level are the same. This implies that Eu^{2+} ions are uniformly distributed across the eight Sr sites with doping levels over 0.5mol%. However, TTSP:Eu^{2+} containing only 0.1mol% of Eu^{2+} shows a slightly shorter emission peak wavelength (see Fig. 4).

The excitation spectrum monitored at 680 nm comprises three main absorption peaks located around 280, 320, and 450 nm. Having a main absorption around 450 nm, which enables it to match to blue LEDs, is exceptional in phosphate phosphors. When comparing excitation spectra among TTSP:Eu^{2+}, α-$Sr_2P_2O_7$:Eu^{2+} and α-$Sr_3(PO_4)_2$:Eu^{2+}, only TTSP:Eu^{2+} can be excited by the blue LED. In the chemical formula, $Sr_4(PO_4)_2O$:Eu^{2+} contains isolated O^{2-} ions whereas α-$Sr_2P_2O_7$:Eu^{2+} and α-$Sr_3(PO_4)_2$:Eu^{2+} do not. Isolated O^{2-} ions, as found in SrO:Eu^{2+} and CaO:Eu^{2+}, are more polarizable than O^{2-} ions in PO_4 and we believe that this structural feature is responsible for the large centroid shift which enables TTSP:Eu^{2+} to be excited in the blue,[18] consistent with the optical properties of TTCP:Eu^{2+}.[6]

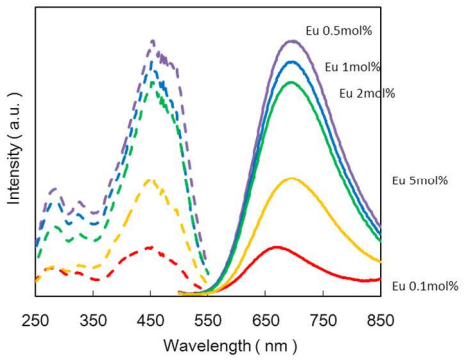

Fig. 3 PL (solid lines) and PLE (dashed lines) spectra of TTSP activated with different concentrations of Eu^{2+}, excited at 465 nm and monitored for 680 nm emission at room temperature.

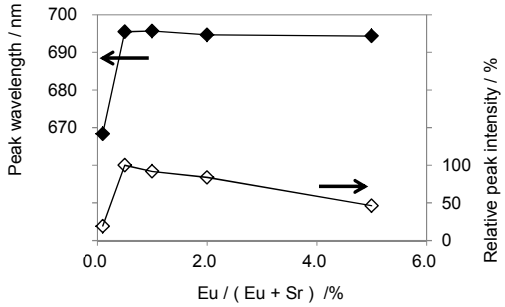

Fig. 4 Emission peak wavelength and relative peak intensity of TTSP:Eu^{2+} as a function of Eu concentration.

3.3.1 The comparison of PL / PLE at room temperature between TTSP:Eu^{2+} and TTCP:Eu^{2+}

Fig. 5 shows the PL and PLE spectra for TTSP:Eu^{2+} at 0.5mol% doping with respect to Sr, compared with TTCP:Eu^{2+} at room temperature. The emission color of TTSP:Eu^{2+} is deep red, which is very similar to the PL of TTCP:Eu^{2+}. The excitation range is also very similar. As shown in Table 1, the lattice volume of TTSP is larger than that of TTCP and a significantly shorter emission peak wavelength from TTSP:Eu^{2+} is expected against TTCP:Eu^{2+} due to the weaker crystal fields on the Eu^{2+} ions in the Sr sites. In simpler structures, SrO has a larger lattice volume, with a Sr-O bond length of 2.58 Å, than CaO with a Ca-O bond length of 2.40 Å; accordingly, an emission peak wavelength of 625 nm was reported for SrO:Eu^{2+},[19] whereas it was 733 nm for CaO:Eu^{2+}.[20] This is the typical case for the relationship between the lattice volume and the emission wavelength being affected by the crystal fields on the cation sites. We have therefore more closely analyzed the detailed link between the structure and the emission performance by comparison of TTSP:Eu^{2+} and TTCP:Eu^{2+} to enhance our understanding of the unique properties of these materials, particularly the differences in the coordination environments of the cation sites between TTSP and TTCP. When discussing metal sites heavily distorted from ideal symmetry, the idea of ECoN is useful.[21] ECoN was introduced in our previous work to deal with structures containing highly distorted coordination polyhedron.[6] ECoN is defined as the sum of the bond weights, which is calculated from the each bond length and the smallest bond length in the coordination polyhedra.[21, 22] Fig. 6 compares the coordination environments around cation sites for TTSP and TTCP in terms of average bond length(a), shortest bond length(b) and ECoNs(c), with sites in the two materials paired by the order of their values rather than crystallographic site. Due to the expansion of the lattice volume, the average bond lengths and the shortest bond lengths of TTSP are significantly longer than for TTCP, which is typically expected to lead to weaker crystal field splitting. However the distortion around the Eu^{2+} ions and the polarizability of O^{2-} ions can also be crucial in determining the emission color. The isolated O^{2-} ions played an important role in achieving a large red shift in TTCP:Eu^{2+}, combined with the distortions of the polyhedra enabling the isolated O^{2-} ions to get closer to the Eu^{2+} ions.

ECoN decreases its value as the shortest bond length becomes smaller, and the shortest bond has an influence on the

distortion of the coordination polyhedra. The eight Sr sites in TTSP have ECoN values ranging from 4.42 to 6.42, depending on the distortion, while the coordination numbers evaluated from bond valence sum are six or seven. Normally the site with the smaller value of the coordination number is more compressed and this places higher chemical pressure on the dopant. Taking into account the deviation in bond lengths from the average, ECoN can therefore indicate the degree of distortion and stress in the polyhedron. When one cation site has a smaller ECoN in TTSP or TTCP, the Eu^{2+} ion in that site can feel a stronger crystal field than in larger ECoN sites. It can be linked to the site that can show longer wavelength emission. As shown in Fig. 6(c), the degrees of the distortion around the cation sites described by ECoN, between TTSP and TTCP, are almost equivalent, which helps to explain their similar emission spectra. A link between the more distorted coordination polyhedra and longer emission wavelength in Ce^{3+} ions has already been shown in the garnet structure.[23]

Another interesting model for large red shifts has been discussed regarding the distortion in $Ca_{3-x}Sr_x(PO_4)_2:Eu^{2+}$.[24] $Sr_2Ca(PO_4)_2:Eu^{2+}$ has a lattice volume of 3843 $Å^3$ and exhibits an emission peak wavelength at 527 nm, while β-$Ca_3(PO_4)_2:Eu^{2+}$ with a smaller unit cell volume of 3533 Å showed a shorter emission peak wavelength at 416 nm. In their discussions, larger neighbouring-cations decrease Eu–O bond lengths as a result of higher stress when larger cations replaced smaller ions. That results in strengthening the Eu^{2+} crystal field splitting, generating the red-shifts. This idea can be extended to the comparison between $TTSP:Eu^{2+}$ and $TTCP:Eu^{2+}$. When comparing neighbouring-cations between Sr and Ca site, larger Sr^{2+} ions as neighbouring-cations can enhance the distortion around an Eu^{2+} ion sitting on a Sr site by displacing the O^{2-} ion from the average position. This is difficult to observe from the average structure obtained from Rietveld refinements, and the low Eu doping concentration also makes it difficult to analyze such local distortions by diffraction-based pair-distribution function techniques.

The polarizability can also have a strong effect on the emission characteristics and the anion polarizability correlates strongly with the cation electronegativity.[25] A plot of the anion polarizability against the inverse square of the cation electronegativity shows a good linearity in oxides. When the cation electronegativity decreases, the polarizability of the anion increases. According to this, the isolated O^{2-} ion is more polarizable than O^{2-} in PO_4. Likewise the O^{2-} ions, which are coordinated by the Sr^{2+} ions, are more polarizable than the O^{2-} ions adjacent to Ca^{2+} ions, since the electronegativity of Sr(0.95) is smaller than Ca(1.0).[26]

In some cases, having the larger ions with smaller electronegativity as neighbouring-cations in a distorted polyhedron can be more important than having smaller average bond lengths to generate the red-shifts.

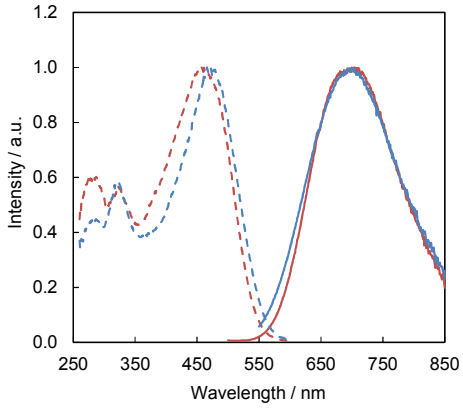

Fig. 5 PL (solid line) and PLE (dashed line) spectra of TTSP with 0.5% of Eu^{2+} (red) and TTCP with 0.5% of Eu^{2+} (blue), excited at 465 nm and monitored for 700 nm emission at room temperature.

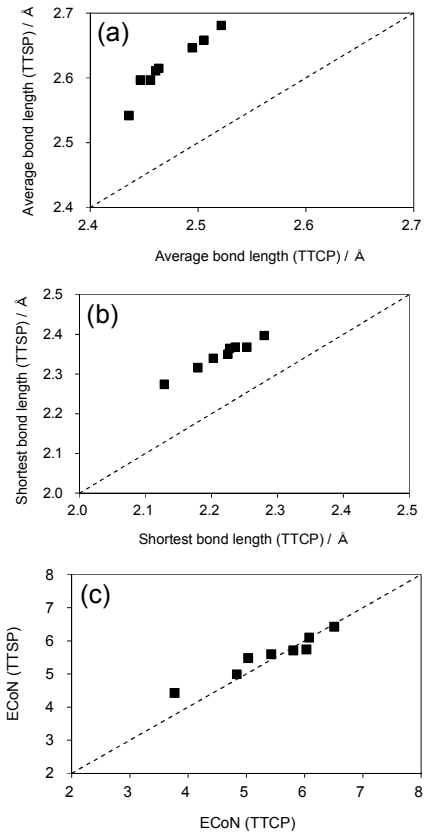

Fig. 6 Comparison of each environment around divalent cation between TTSP and TTCP, average bond length(a), shortest bond length(b) and ECoN(c).

3.3.2 The comparison of PL / PLE at 77 K between $TTSP:Eu^{2+}$ and $TTCP:Eu^{2+}$

Fig. 7 shows the comparison of PL and PLE between $TTSP:Eu^{2+}$ and $TTCP:Eu^{2+}$ at 77 K. $TTCP:Eu^{2+}$ has a yellow emission component at around 560 nm, being excited by 465 nm light at 77 K. However, as the temperature increases to ambient conditions the emission shoulder at around 560 nm

decreases its peak intensity rapidly, showing much stronger thermal quenching than at around 670 nm. This is the opposite of what would be expected from the conventional idea of the configurational coordinate diagram (CCD), wherein thermal quenching of PL become stronger when the transversal offset between the ground-state parabola and the excited state parabola becomes larger, leading to stronger thermal quenching of longer emission wavelengths.[27] In the case of TTSP:Eu^{2+}, it interestingly emits only red light at 77 K. A comparison of the thermal behavior of TTSP:Eu^{2+} and TTCP:Eu^{2+}, in particular their possible energy diagrams, is important for the key factors responsible for the thermal quenching to be understood.

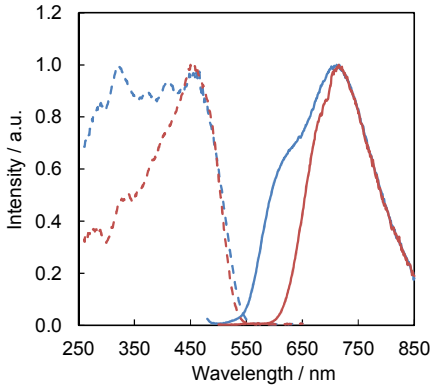

Fig. 7 PL (solid line) and PLE (dashed line) spectra of TTSP:Eu^{2+} (red) and TTCP:Eu^{2+} (blue), excited at 465 nm and monitored for 700 nm emission at 77 K.

The diffuse reflection spectra of Eu-doped TTSP and TTCP were measured and their absorption spectra (K/S) derived with the Kubelka - Munk function (1) are shown in the Fig. 8. The Kubelka - Munk function is defined as:

$$F(R) = (1\text{-}R)^2 / 2R = K/S \quad (1)$$

where R, K and S are the reflection, the absorption and the scattering coefficients, respectively. TTSP:Eu^{2+} showed a quite similar absorption curve to TTCP:Eu^{2+}. It increases the absorption in the range of 3 - 5 eV associated with the energy transition from the $4f^7(^8S_{7/2})$ ground state to the $4f^6 5d^1$ excited state of the Eu^{2+} ions, and the sudden rise around 5.5 eV corresponds to the absorption at the band gap of TTSP. This confirms that the crystal field environment around Eu^{2+} in the TTSP structure is very similar to the one in the TTCP structure. The value of the optical band gap can be calculated by extrapolating the Kubelka - Munk function $F(R)$ to $K/S = 0$.[28] This gave a value of the optical band gap in the Eu-doped TTSP, Eg, of about 5.5 eV for TTSP and 6.2 eV for TTCP, which appears sufficiently close to the computed band gap of 5.47 eV for TTSP and 6.12 eV for TTCP. The calculated Densities of States (DOSs) from TTSP and TTCP are shown in Fig. 9. According to Ref. 29, the calculation of band gaps based on the HSE agreed well with the experimental values up to around 6 eV, within a 0.5 eV deviation. The band gap differences between TTSP and TTCP are 0.7 eV from the experiment and 0.65 eV from the calculation, respectively. Thus, around 0.7 eV of energy difference in the band gap is assumed.

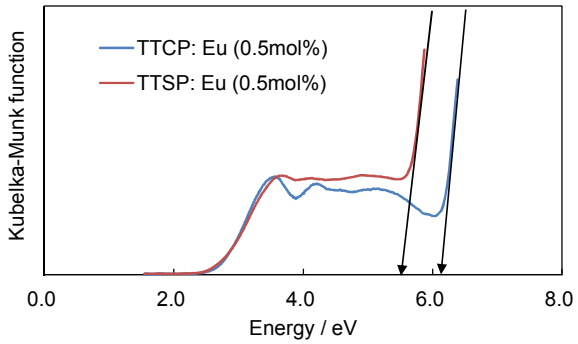

Fig. 8 Absorption spectra of TTSP:Eu^{2+} (red) and TTCP:Eu^{2+} (blue).

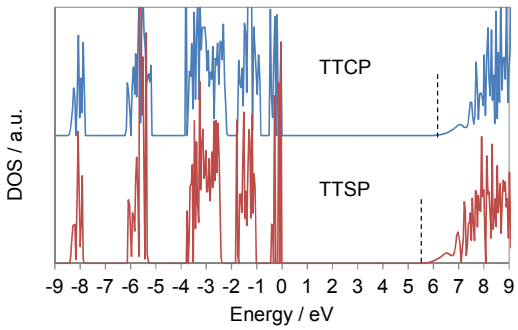

Fig. 9 Calculated DOSs of TTSP (red) and TTCP (blue). The vertical dashed bars indicate the end of the fundamental band gap.

The stronger thermal quenching of shorter wavelength emission can be explained on the basis of auto-ionization from the 5*d* level of Eu^{2+} to the conduction band, as discussed in the $SrAl_2O_4$:Eu^{2+},Dy^{3+} phosphor,[30] wherein the blue emission has stronger thermal quenching (little luminescence at room temperature) than green emission. Similarly, the degree of auto-ionization can be considered on each Sr and Ca site. The schematic energy diagram for TTCP:Eu^{2+} was suggested in our previous work to explain the different thermal quenching behavior representing two typical sites with the yellow emission at the peak position of 560 nm being excited by 346 nm and the red emission at the peak position of 670 nm being excited by 466 nm, as shown in Fig. 10(b).[6] A smaller energy gap between the 5*d* energy level of Eu^{2+} and the bottom of conduction band on the 560 nm emission site should therefore be expected compared to the 670 nm emission site. These energy gaps between the 5*d* energy levels of Eu^{2+} and the bottom of conduction band on each emission site can affect the degree of auto-ionization. Considering the PLE and absorption spectra of TTSP:Eu^{2+} and TTCP:Eu^{2+}, it is assumed that *inert* 4*f* ground states and excited 5*d* levels of each Eu^{2+} in both TTSP and TTCP structure locate at more or less the same energy level in the band gap. The evaluated band gaps of TTSP:Eu^{2+} and TTCP:Eu^{2+} from the Kubelka-Munk function are about 5.5 eV and 6.2 eV, respectively.

The thermal excitation of the 5*d* electron to the conduction band states was suggested as an intrinsic mechanism.[31] As shown in their empirical formula, $\Delta E = T_{0.5}/680$ eV, where $T_{0.5}$ is the quenching temperature at which the emission intensity

has dropped to 50% of the low temperature value and ΔE is the energy barrier, a sub-eV difference may be significant for thermal quenching. The energy difference of the band gap between TTSP and TTCP is about 0.7 eV, which corresponds to the quenching temperature difference of 476 K. This can be a crucial factor to make the energy relaxation process non-radiative on the shorter emission of TTSP:Eu^{2+}. This explains why, unlike in TTCP:Eu^{2+}, several of the sites do not appear to contribute to the emission spectra.

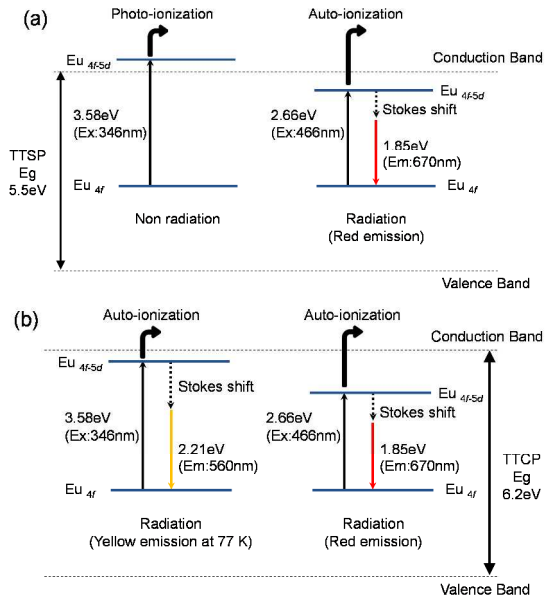

Fig. 10 Schematic energy diagram of TTSP:Eu^{2+}(a) and TTCP:Eu^{2+}(b) representing yellow emission (560 nm) and red emission (670 nm).

4 Conclusions

The new red phosphor $Sr_4(PO_4)_2O:Eu^{2+}$ is reported. It shows a broad deep red emission with a peak position at 680 nm being excited at around 450 nm, which matches well with blue LEDs. The crystal structure of $Sr_4(PO_4)_2O:Eu^{2+}$ was refined in a monoclinic $P2_1$ structure. It is isotypic to $Ca_4(PO_4)_2O:Eu^{2+}$, which also shows deep red emission. Their emission and excitation spectra at room temperature are very similar despite $Sr_4(PO_4)_2O:Eu^{2+}$ having a much larger unit cell volume than $Ca_4(PO_4)_2O:Eu^{2+}$. The relationship between the crystal structure and the emission spectra of $Sr_4(PO_4)_2O:Eu^{2+}$ was discussed by comparison with $Ca_4(PO_4)_2O:Eu^{2+}$ to find the key factors for achieving a large redshift of the 5*d* level of Eu^{2+} ion to emit red light. The importance of the anion polarizability and the distortion of the coordination polyhedron were highlighted based on the idea of the electronegativity of the cations and the ECoNs. $Ca_4(PO_4)_2O:Eu^{2+}$ shows yellow emission at 77 K, whereas $Sr_4(PO_4)_2O:Eu^{2+}$ does not. The different thermal quenching behaviors for Eu^{2+} dopants in $Sr_4(PO_4)_2O:Eu^{2+}$ and $Ca_4(PO_4)_2O:Eu^{2+}$ were also discussed and attributed to the degree of auto/photo-ionization caused by the different band gaps of the materials. The importance of the large band gap of the host lattice in avoiding non-radiative processes of energy relaxation was confirmed.

Acknowledgements

The authors thank Dr Ali Kalaji for his assistance with the experimental work at the University of Cambridge. The authors are also grateful to Dr Chiu Tang and Dr Stephen Thompson for their help with the data collection on beamline I11 at the Diamond Light Source facility in the UK. (Beamtime proposal number: EE7854-1). PJS thanks the Glasstone Trust for funding via a fellowship.

Notes and references

[a] Mitsubishi Chemical Corporation, 1060 Naruda, Odawara, Kanagawa 250-0862, Japan
[b] MCHC R&D Synergy Center, Inc., 1000 Aoba, Kamoshida, Yokohama, Kanagawa 227-8502, Japan
[c] University of Oxford, Inorganic Chemistry Laboratory, South Parks Road, Oxford OX1 3QR, UK
[d] University of Tsukuba, Institute of Applied Physics, 1-1-1 Tennoudai, Tsukuba, Ibaraki 305-8573, Japan
[e] University of Cambridge, Department of Materials Science and Metallurgy, 27 Charles Babbage Road, Cambridge CB3 0FS, UK

1 S. Nakamura, S. Pearton and G. Fasol, The Blue Laser Diode : The Complete Story, pp. 230-235, Springer-Verlag, Berlin 2000.
2 J. McKittrick, M. E. Hannah, A. Piquette, J. K. Han, J. I. Choi, M. Anc, M. Galvez, H. Lugauer, J. B. Talbot and K. C. Mishra, *ECS J. Solid State Sci. Technol.*, 2013, **2**, R3119.
3 C. C. Lagos, *J. Electrochem. Soc.: SOLID STATE SCIENCE*, 1970, **117**, 1189.
4 J. C. Zhang, Y. Z. Long, H. D. Zhang, B. Sun, W. P. Han and X. Y. Sun, *J. Mater. Chem. C*, 2014, **2**, 312.
5 N. Komuro, M. Mikami, Y. Shimomura, E. G. Bithell and A. K. Cheetham, *J. Mater. Chem. C*, 2014, **2**, 6084.
6 N. Komuro, M. Mikami, P. J. Saines and A. K. Cheetham, *J. Lumin.*, 2015, **162**, 25.
7 E. R. Kreidler and F. A. Hummel, *Inorg. Chem.,* 1967, **6**, 884.
8 S. P. Thompson, J. E. Parker, J. Potter, T. P. Hill, A. Birt, T. M. Cobb, F. Yuan, and C. C. Tang, *Rev. Sci. Instrum.,* 2009, **80**, 075107.
9 A.C. Larson and R. B. Von Dreele, "General Structure Analysis System (GSAS)", Los Alamos National Laboratory Report LAUR 86-748, 1994.
10 B. H. Toby, *J. Appl. Crystallogr.*, 2001, **34**, 210.
11 K. Momma and F. Izumi, *J. Appl. Crystallogr.*, 2011, **44**, 1272.
12 G. Kresse and J. Furthmuller, *Phys. Rev. B,* 1996, **54**, 11169.
13 G. Kresse and D. Joubert, *Phys. Rev. B,* 1999, **59**, 1758.
14 A. V. Krukau, O. A. Vydrov, A. F. Izmaylov and G. E. Scuseria, *J. Chem. Phys.,* 2006, **125**, 224106.
15 H. Bauer and W. Balz, *Z. Anorg. Allg. Chem.*, 1965, **340**, 225.
16 Q. Guo, L. Liao, L. Mei and H. Liu, *J. Solid State Chem.*, 2015, **226**, 107.
17 R. E. Brese and M. O'Keeffe, *Acta Crystallogr. Sect. B,* 1991, **B47**, 192.
18 M. Mikami, *ECS J. Solid State Sci. Technol.* 2013, **2**, R3048.
19 N. Yamashita, *J. Lumin.* 1994, **59**, 195.
20 N. Yamashita, *J. Electrochem. Soc.,* 1993, **140**, 840.

21 M. Nespolo, G. Ferraris, G. Ivaldi and R. Hoppe, *Acta Crystallogr., Sect. B: Struct. Sci.,* 2001, **57**, 652.
22 R. Hoppe, S. Voigt, H. Glaum, J. Kissel, H. P. Muller and K. Bernet, *J. Less-Common. Met.*, 1989, **156**, 105.
23 G. Gundiah, J. L. Wu and A. K. Cheetham, *Chem. Phys. Lett.,* 2007, **441**, 250.
24 H. Ji, Z. Huang, Z. Xia, M. S. Molokeev, V. V. Atuchin, M. Fang and Y. Liu, *J. Phys. Chem. C,* 2015, **119**, 2038.
25 P. Dorenbos, *Phys. Rev. B,* 2002, **65**, 235110.
26 A. L. Allred, *J. Inorg. Nucl. Chem.*, 1961, **17**, 215.
27 G. Blasse and B. C. Grabmaier, Luminescent Materials, Springer, Berlin, 1994.
28 C. J. Duan, A. C. A. Delsing and H. T. Hintzen, *Chem. Mater.,* 2009, **21**, 1010.
29 F. Tran and P. Blaha, *Phys. Rev. Lett.,* 2009, **102**, 226401.
30 J. Ueda, T. Nakanishi, Y. Katayama and S. Tanabe, *Phys. Status Solidi C,* 2012, **9**, 2322.
31 P. Dorenbos, *Condens. Matter,* 2005, **17**, 8103.

